



A Journal of



Accepted Article

Title: Tyrosinase model systems supported by pyrazolylmethylpyridine ligands: electronic and steric factors influencing the catalytic activity and impact of complex equilibria in solution

Authors: Benjamin Herzigkeit, Benedikt Maria Flöser, Tobias Adrian Engesser, Christian Näther, and Felix Tuczec

This manuscript has been accepted after peer review and appears as an Accepted Article online prior to editing, proofing, and formal publication of the final Version of Record (VoR). This work is currently citable by using the Digital Object Identifier (DOI) given below. The VoR will be published online in Early View as soon as possible and may be different to this Accepted Article as a result of editing. Readers should obtain the VoR from the journal website shown below when it is published to ensure accuracy of information. The authors are responsible for the content of this Accepted Article.

To be cited as: *Eur. J. Inorg. Chem.* 10.1002/ejic.201800319

Link to VoR: <http://dx.doi.org/10.1002/ejic.201800319>

WILEY-VCH

Tyrosinase model systems supported by pyrazolylmethylpyridine ligands: electronic and steric factors influencing the catalytic activity and impact of complex equilibria in solution

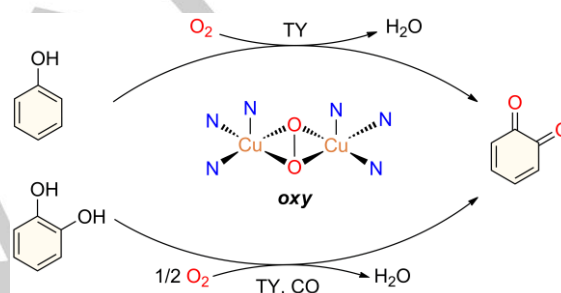
Benjamin Herzigkeit,^[a] Benedikt M. Flöser,^[a] Tobias A. Engesser,^[a] Christian Näther^[a] and Felix Tuczek*^[a]

Dedicated to Prof. Dr. Peter Comba on the occasion of his 65th anniversary

Abstract: Two new copper(I) complexes supported by pyrazolylmethylpyridine (**PMP**) ligands are synthesized and investigated regarding their ability to catalyze the oxygenation of several monophenolic substrates. The **PMP** ligands containing a pyridine and a pyrazole donor group represent hybrids between dipyrldimethane (**DPM**) and bispyrazolylmethane (**BPM**) ligands. The catalytic activity of the two new $[\text{Cu}(\text{MeCN})_2\text{PMP}]\text{PF}_6$ complexes is found to be intermediate between that of catalytically inactive $[\text{Cu}(\text{MeCN})_2\text{DPM}]\text{PF}_6$ and highly active $[\text{Cu}(\text{MeCN})_2\text{BPM}]\text{PF}_6$, suggesting that the electronic properties of a multidentate ligand can be designed in a modular fashion. DFT calculations are used to explore the differences in reactivity between the two systems. Regarding the behaviour of these complexes in solution, evidence for an equilibrium between homoleptic and heteroleptic forms is presented. The crystal structure of a dinuclear complex exhibiting two homoleptic Cu(II) units bridged by a fluorido ligand is obtained, which might represent one of the decay products of **PMP**-type catalysts after prolonged reaction times.

Introduction

Melanin, an ubiquitous biopolymer, is involved in many pigmentation processes.^[1] It plays a major role in skin protection from UV light or ionizing radiation^[2], in wound healing, immune response^[3], the coloring of hair and skin^[4] and browning of fruits and vegetables.^[5] In melanogenesis tyrosinase (TY) catalyzes the conversion of the amino acid L-tyrosine to L-DOPAquinone through a two-step reaction combining a hydroxylation and a subsequent two-electron oxidation.^[6-8] Catechol oxidase (CO), with a very similar active site, is only able to perform the oxidation step (Scheme 1).^[6-9] TY and CO are both copper type 3 enzymes



Scheme 1. Reactions performed by tyrosinase (TY) and catechol oxidase (CO). Centre: Schematic drawing of the oxy-form of the active site.

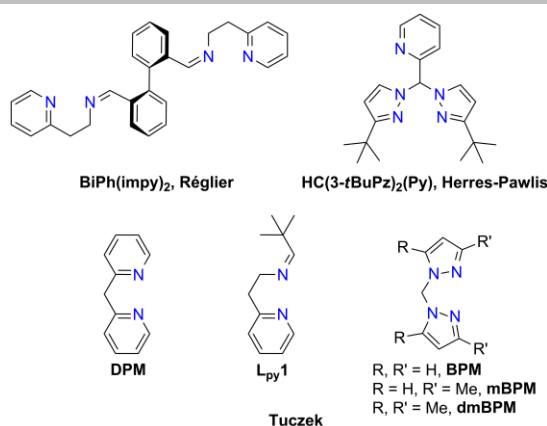
which bind dioxygen as peroxide between the copper centers in a typical side-on bridging geometry ($\mu\text{-}\eta^2\text{:}\eta^2$) (**oxy**, Scheme 1).^[7-9] This characteristic feature was also confirmed by the first X-ray crystal structure of tyrosinase from the bacterium *Streptomyces castaneoglobosporus*.^[10] Since then, more and more crystal structures of polyphenol oxidases (PPOs) were obtained from bacteria, insects and plants, revealing subtle structural differences between the various organisms.^[11-13]

Small changes in the structure of the active site often have a major impact on the function of the enzyme. The same applies to the numerous and diverse small-molecule models of tyrosinase and catechol oxidase (Scheme 2).^[6-9,14-17] One of the first model systems capable of catalytically oxygenating 2,4-di-*tert*-butylphenol (2,4-DTBP-H) to 3,5-di-*tert*-butylquinone (3,5-DTBQ) was the complex $[\text{Cu}_2(\text{MeCN})_4\text{BiPh}(\text{impy})_2](\text{PF}_6)_2$ developed by Réglier *et al.*^[18] Since then the number of model systems has significantly increased, showing that small variations in ligand design can give rise to large differences in catalytic activity.^[19-22] In 2010, our group presented the complex $[\text{Cu}(\text{MeCN})_2\text{L}_{\text{py}}\mathbf{1}]\text{PF}_6$ supported by the mononucleating pyridine-imine ligand **L_{py}1** as a catalyst for the tyrosinase-like *ortho*-oxygenation of 2,4-DTBP-H to 3,5-DTBQ.^[18,23] Afterwards, we exchanged the pyridine moiety of **L_{py}1** for different heterocyclic groups (i.e. pyrazoles or benzimidazole). In comparison to the parent complex, the Cu(I) complexes derived from the resulting ligands showed similar and even enhanced (up to a turnover number of 31) catalytic activities.^[24] By replacing the imine and pyridine function with two pyrazoles, leading to the **BPM**, **mBPM**, **dmBPM** systems

[a] Institut für Anorganische Chemie, Christian-Albrechts-Universität zu Kiel, Max-Eyth-Straße 2, 24118 Kiel, Germany
E-mail: ftuczek@ac.uni-kiel.de
<http://www.ac.uni-kiel.de/tuczek>

Supporting information for this article is given via a link at the end of the document.

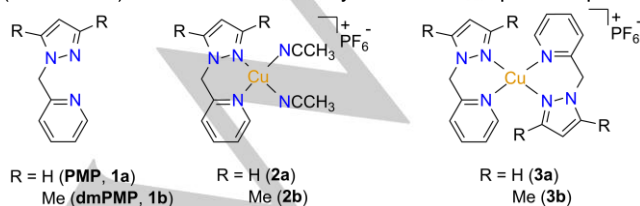
FULL PAPER



Scheme 2. Mono- and binucleating ligands included in model complexes for the oxygenation of various substrates in a tyrosinase-like fashion.^[18, 18, 26, 27]

(Scheme 2), the same catalytic activities as in the case of the **L_{py}1** containing system were observed.^[25] On the other hand, replacement of an imine with an oxazoline as a second donor led to a total loss of catalytic tyrosinase activity, with only catecholoxidase activity remaining.^[26] Likewise, no catalytic tyrosinase activity was observed with a dipyrildimethane system (**DPM**).^[23] In view of the catalytically active **BPM** systems and the (equally active) **HC(3-*t*BuPz)₂(Py)** complex developed 2013 by Herres-Pawlis *et al.*, which is supported by a ligand containing one pyridine and two *tert*-butyl-substituted pyrazoles per copper center, the presence of one or more pyrazole moieties seems to positively influence the catalytic activity of the derived Cu(I) complexes.^[25, 27] Therefore, we decided to replace the imine function in **L_{py}1** with a pyrazole to obtain the new ligands **1a** (**PMP**) and **1b** (**dmPMP**) (Scheme 2), which had already shown interesting properties when coordinated to several transition metals, but have not been investigated with regard to copper oxygenation chemistry yet.^[28-30] The influence exerted by this bidentate ligand combining a soft (pyridine N) and hard (pyrazole N) donor on the coordination chemistry and the catalytic activity of derived copper complexes should provide useful information for further ligand and catalyst design.

Herein we present the synthesis of cationic hetero- and homoleptic complexes of the type $[\text{Cu}(\text{MeCN})_2\text{L}]^+$ and $[\text{CuL}_2]^+$ (**L** = **PMP**, **dmPMP**; Scheme 3). Detailed structural and theoretical studies are performed in order to elucidate the physicochemical properties and the coordination behavior of the obtained compounds in solution. Furthermore, the catalytic activities of the heteroleptic copper(I) complexes $[\text{Cu}(\text{MeCN})_2\text{PMP}]\text{PF}_6^-$ (**2a**) and $[\text{Cu}(\text{MeCN})_2\text{dmPMP}]\text{PF}_6^-$ (**2b**) regarding the oxygenation of 2,4-DTBP-H, 3-*tert* butylphenol (3-TBP-H) and 4-methoxyphenol (4-MeOP-H) as well as the activity of the homoleptic complexes



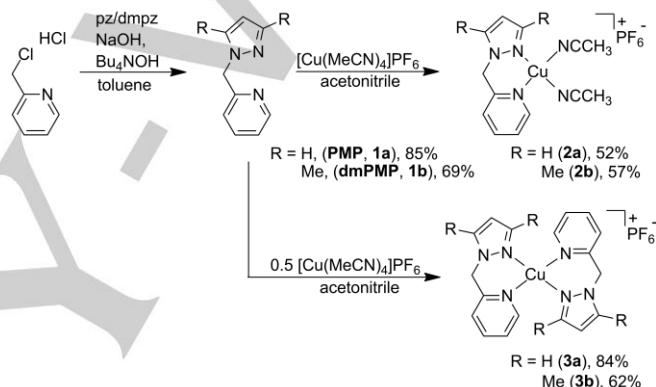
Scheme 3. Pyrazolylmethylpyridine ligands (**1a**, **1b**) and their heteroleptic (**2a**, **2b**) and homoleptic Cu(I) complexes (**3a**, **3b**) investigated in this study.

$[\text{Cu}(\text{PMP})_2]\text{PF}_6^-$ (**3a**) and $[\text{Cu}(\text{dmPMP})_2]\text{PF}_6^-$ (**3b**) regarding the oxygenation of 2,4-DTBP-H are examined. The results are discussed and compared with those obtained on previous small-molecule models of tyrosinase supported by bidentate ligands.

Results and Discussion

Synthesis of the ligands and their copper(I) complexes

The two ligands **1a** and **1b** were synthesized according to the procedure of House *et al.*^[29] In a phase-transfer catalysis with Bu_4NOH 2-picoyl chloride hydrochloride was alkylated with the corresponding pyrazole (Scheme 4). For the work-up of the respective ligands we deviated from the original procedure (see Exp. Sect.). Both ligands were converted to their corresponding hetero- (**2a**, **2b**) and homoleptic (**3a**, **3b**) copper(I) complexes under anaerobic conditions employing tetrakis(acetonitrile)-copper(I) hexafluorophosphate (for more details see Exp. Sect.).

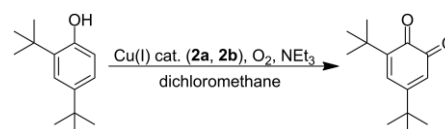


Scheme 4. Syntheses of the ligands (**PMP**, **1a** and **dmPMP**, **1b**) and the hetero- (**2a**, **2b**) and homoleptic (**3a**, **3b**) copper(I) complexes. Pz = 1*H*-pyrazole; dmpz = 3,5-dimethylpyrazole.

Tyrosinase activity of **2a** and **2b**

For the detection of a catalytic tyrosinase activity of the heteroleptic complexes **2a** and **2b** we chose the three monophenolic substrates 2,4-DTBP-H, 3-TBP-H and 4-MeOP-H exhibiting different structural and electronic properties. The sterically most demanding monophenol 2,4-DTBP-H was used because of the formation of its stable *ortho*-quinone 3,5-DTBQ (Scheme 5), whereas the less congested monophenols 3-TBP-H and 4-MeOP-H form characteristic secondary products (see below).

First, we checked the catalytic tyrosinase activity of **2a** and **2b** with the substrate 2,4-DTBP-H (Scheme 5). The oxygenation was carried out under Bulkowski/Réglier conditions in all cases.^[18,31] To this end, a 500 μM solution of the copper(I) catalyst in dichloromethane was prepared and 50 equivalents 2,4-



Scheme 5. Catalytic reaction of the phenolic substrate 2,4-DTBP-H to *ortho*-quinone 3,5-DTBQ.

FULL PAPER

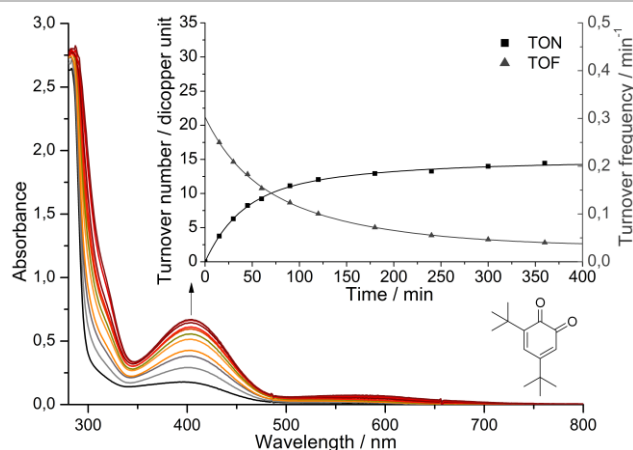
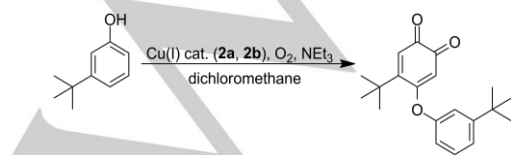


Figure 1. UV/vis spectra measured during the catalytic oxygenation of a 500 μM solution of $[\text{Cu}(\text{MeCN})_2\text{PMP}]\text{PF}_6$ (**2a**) in dichloromethane in the presence of 2,4-DTBP-H (50 equiv.) and triethylamine (100 equiv.) during the first 6 h at room temperature; quartz cell length $l = 1$ mm; inset: Turnover number per dicopper unit (black squares) and turnover frequency per minute (gray triangles) as a function of time.

DTBP-H and 100 equivalents triethylamine per mononuclear complex were added. Oxygenation of the reaction mixture led to the formation of 3,5-DTBQ which was monitored by in situ UV/vis spectroscopy based on the absorption band at 407 nm ($\epsilon = 1830 \text{ L mol}^{-1} \text{ cm}^{-1}$).^[18,23,25] Both complexes are catalytically active with a turnover number (TON) of 14 after 6 h for **2a** and 11 after 7 h per dicopper unit for **2b** (Figure 1, Figure S1). The reaction proceeds fast at the beginning with a high turnover frequency (TOF), but nearly comes to a halt after 4 h for both complexes (Figure 1, inset, Figure S1).

After one hour of oxygenation an aliquot was removed from the reaction mixture and diluted to a 100 μM solution in dichloromethane, which was treated with 6 M hydrochloric acid to remove any copper species. After extraction and removal of solvent ^1H - and ^{13}C -NMR spectra were measured (cf. Figure S2, S3) in order to identify the organic catalysis products. According to the ^1H -NMR spectrum of the aliquot of **2a** 79% of the starting material 2,4-DTBP-H, 11% of the C-C coupling product 3,3',5,5'-tetra-*tert*-butyl-2,2'-biphenol (biphenol) and 10% of 3,5-DTBQ are present after 1 h of oxygenation (Table S1), which is also in agreement with the UV/vis spectra (TON = 9) after 1 h (cf. Figure 1). Application of the same protocol to the methyl-substituted system **2b** resulted in a distribution of 87% 2,4-DTBP-H, 7% biphenol and 6% 3,5-DTBQ (cf. Figure S4, S5, Table S1). These results indicate that both heteroleptic copper(I) complexes are catalytically active towards the conversion of 2,4-DTBP-H to 3,5-DTBQ.

To investigate a sterically less crowded substrate 3-*tert*-butylphenol (3-TBP-H) was employed (Scheme 6). In comparison with 2,4-DTBP-H it has no *tert*-butyl group in direct vicinity of the



Scheme 6. Catalytic reaction of the substrate 3-TBP-H to 4-(*tert*-butyl)-5-(3-(*tert*-butyl)phenoxy)cyclohexa-3,5-diene-1,2-dione.

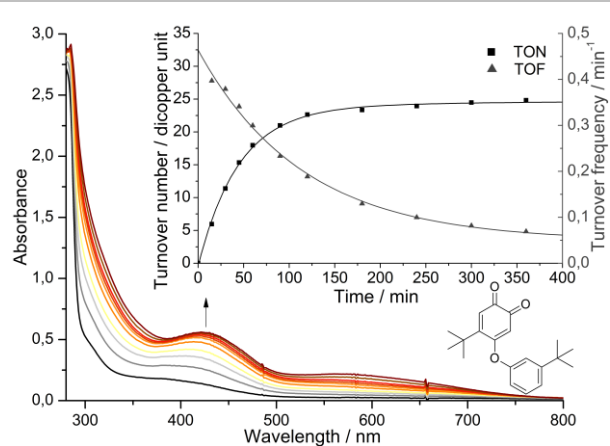
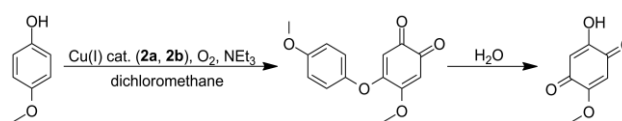


Figure 2. UV/vis spectra measured during the catalytic oxygenation of a 500 μM solution of $[\text{Cu}(\text{MeCN})_2\text{PMP}]\text{PF}_6$ (**2a**) in dichloromethane in the presence of 3-TBP-H (50 equiv.) and triethylamine (100 equiv.) during the first 6 h at room temperature; quartz cell length $l = 1$ mm; inset: Turnover number per dicopper unit (black squares) and turnover frequency per minute (gray triangles) as a function of time.

hydroxy function and the remaining *tert*-butyl group is located in *meta* position, which reduces the stability of the *ortho*-quinone product towards further reactions. Correspondingly, after initial formation of an absorption band at ~ 400 nm for 4-*tert*-butylquinone, an oxidative coupling to 4-(*tert*-butyl)-5-(3-(*tert*-butyl)phenoxy)cyclohexa-3,5-diene-1,2-dione occurs, as evident from the shift of the absorption band to 425 nm.^[22,32] For complex **2a** a TON of 25 for the oxidatively coupled product ($\epsilon = 898 \text{ L mol}^{-1} \text{ cm}^{-1}$) was achieved after 6 h of oxygenation at room temperature (Figure 2).^[26] Sterically more encumbered **2b** led to a TON of 13 after 4 h; afterwards no further increase of the absorption band was observable (Figure S6). Regarding the TOF of both complexes the fastest rate was observed directly at the start of the oxygenation after which it rapidly decreased (Figure 2, inset). ^1H -NMR of a quenched aliquot of the reaction mixture after 1 h revealed the ratio between starting material 3-TBP-H and coupled *ortho*-quinone to be 82:18 for **2a** (Figure S7, S8, Table S1) and 89:11 for **2b** (cf. Figure S9, S10, Table S1).

As a third, more electron-rich substrate 4-methoxyphenol (4-MeOP-H) was examined (Scheme 7). This substrate is already known to be oxidized by tyrosinase to 4-methoxy-1,2-benzoquinone.^[33] The electron-donating methoxy group causes an increase of the electron density in the aromatic system and therefore promotes the electrophilic attack of the peroxy core.^[25,26] Moreover, the formed quinone is quite reactive, forming the coupled product 4-methoxy-5-(4-methoxyphenoxy)cyclohexa-3,5-diene-1,2-dione at room temperature which can be monitored by UV/vis (418 nm band, $\epsilon = 524 \text{ L mol}^{-1} \text{ cm}^{-1}$) throughout the catalytic reaction.^[22,26,34] After some time water formed during the reaction hydrolyzes the coupled *ortho*-quinone, converting it into



Scheme 7. Catalytic reaction of the substrate 4-MeOP-H to 4-methoxy-5-(4-methoxyphenoxy)cyclohexa-3,5-diene-1,2-dione and 2-hydroxy-5-methoxy-1,4-benzoquinone.

FULL PAPER

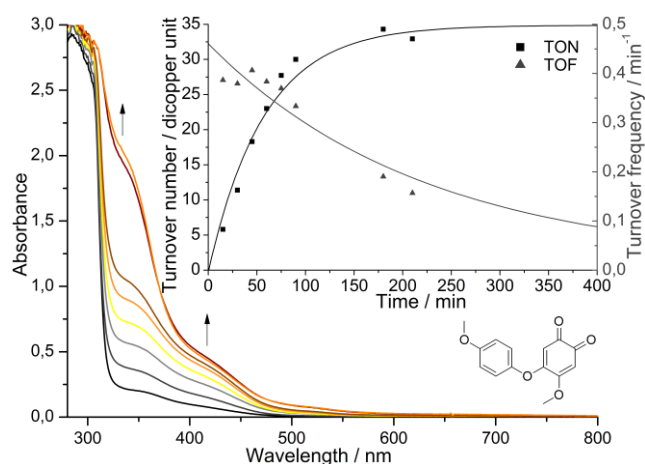
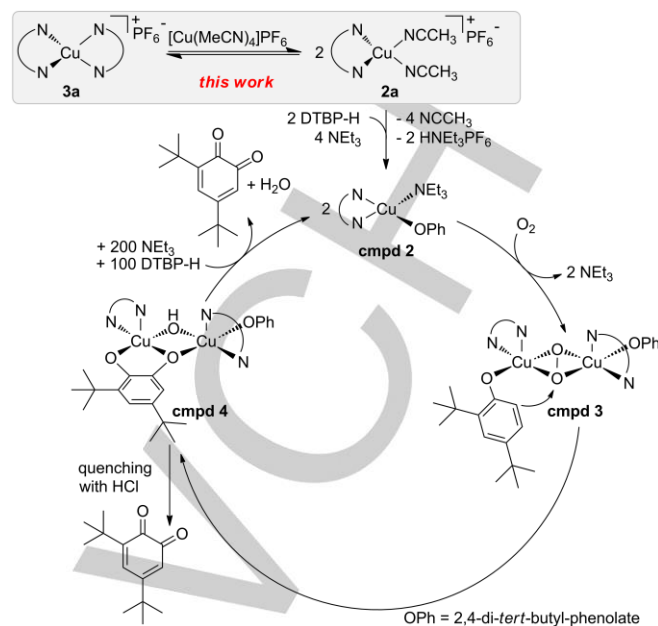


Figure 3. UV/vis spectra measured during the catalytic oxygenation of a 500 μM solution of $[\text{Cu}(\text{MeCN})_2\text{PMP}]\text{PF}_6$ (**2a**) in dichloromethane in the presence of 4-MeOP-H (50 equiv.) and triethylamine (100 equiv.) during the first 3.5 h at room temperature; quartz cell length $l=1$ mm; inset: Turnover number per dicopper unit (black squares) and turnover frequency per minute (gray triangles) as a function of time.

2-hydroxy-5-methoxy-[1,4]-benzoquinone and 4-MeOP-H.^[26] For **2a** a TON of 34 for the oxidatively coupled product 4-methoxy-5-(4-methoxyphenoxy)-cyclohexa-3,5-diene-1,2-dione was observed after 3 h of oxygenation at room temperature (Figure 3), whereas **2b** reached a TON of 33 after 1.5 h (Figure S11). The TOF decreases significantly after 1.5 h of oxygenation for both complexes **2a** and **2b** (Figure 3 inset, S11).

An aliquot of the oxygenation mixture was quenched after 1 and 3 h of reaction time, and the organic products were analysed via ^1H - and ^{13}C -NMR (Figure S12-S15, Table S1). The ^1H -NMR spectrum of **2a** after 1 h showed the coupled *ortho*-quinone and unreacted substrate in a ratio of 22 : 78. The ^1H -NMR spectrum recorded after 3 h indicated a notable increase of coupled *ortho*-quinone. Additionally, the formation of *para*-quinone became measurable, whereby a ratio of 13 % *para*-quinone : 35 % coupling product : 52 % unreacted substrate was determined (cf. Figure S12-S15). For **2b** the ^1H -NMR spectrum recorded after 1 h showed that *para*-quinone was already present, resulting in a ratio of 7 : 38 : 55 (cf. Figure S16, S17). After 3 h the proceeding reactions to the *para*-quinone and presumably the formation of several not identified side-products led to a decrease of coupled *ortho*-quinone (9 : 29 : 62) (cf. Figure S18, S19).

The catalytic cycle of the heteroleptic copper(I) complexes **2a** and **2b** should be similar to the proposed cycle with previously published model systems (Scheme 8).^[23-26] For both complexes **2a** and **2b** we were able to detect a $\mu-\eta^2:\eta^2$ -peroxo intermediate at low temperatures by UV/vis spectroscopy (Figure S20, S21). However, the yield of the peroxo adduct was rather low (2.5% for **2a** and 3.3% for **2b** based on an ϵ value of 20000 $\text{L mol}^{-1}\text{cm}^{-1}$ for



Scheme 8. Proposed catalytic cycle for PMP-based systems in analogy to our previous model systems with the substrate 2,4-DTBP-H. A possible equilibrium prior to the used catalyst **2a** is investigated in this work.

the 349 nm band). This might be attributed to a possible blocking of the coordination site by the two acetonitrile co-ligands.^[37, 36] For an assignment of the absorption bands we performed time-dependent density functional theory (TD-DFT) calculations (Figure S20).

In conclusion it could be shown that the two new heteroleptic complexes **2a** and **2b** are catalytically active towards the three substrates 2,4-DTBP-H, 3-TBP-H and 4-MeOP-H.

Electronic and steric factors influencing catalytic activity

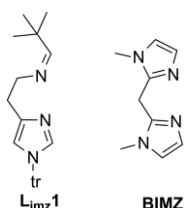
In the past years the range of copper complexes mediating a catalytic tyrosinase-like reaction has been significantly extended.^[8, 22-27, 37] For an assessment of the new systems presented herein, we compare their catalytic activities with a number of similar copper complexes supported by bidentate ligands (Table 1; Scheme 2 and 9). Although not every single system was examined with all substrates, comparison of the data provides some clues that may be relevant for the future design of such systems.

Most of our work focused on the substrate 2,4-DTBP-H. Comparing the new complexes **2a** (14) and **2b** (11) it is notable that **2b** achieves a lower TON. This is analogous to the symmetric pyrazole systems **BPM** and **dmBPM** where the TON is lowered by introducing a methyl group in the vicinity of the heterocyclic N-donor.^[25] Generally a lowering of the TON is observed if the

Table 1. Turnover numbers (TON) for the conversion of several substrates for model systems with a bidentate ligand design.

System	$\text{L}_{\text{py}}1$ [23]	DPM [23]	BPM [25,35]	dmBPM [25,35]	$\text{L}_{\text{imz}}1$ [26]	BIMZ [26]	PMP <i>this work</i>	dmPMP <i>this work</i>
2,4-DTBP-H	22	0	21	11	16	9	14	11
3-TBP-H	-	-	22	12	20	6	25	13
4-MeOP-H	-	-	35	15	34	6	34	33

FULL PAPER



Scheme 9. Structure of the imidazole based ligands L_{imz1} and **BIMZ**.^[26]

copper peroxy adduct is shielded by bulky groups, e.g. in the **HC(3-tBuPz)₂(Py)**-system by Herres-Pawlis or in the **Bustacn**-system by Scarborough.^[27, 38] On the other hand, both **2a** and **2b** achieve lower TONs than $[Cu(MeCN)_2L_{py1}]PF_6$ (**22**) and $[Cu(MeCN)_2L_{imz1}]PF_6$ (**16**; cf Scheme 9) containing combinations of imine and pyridine or imidazole groups, respectively. Regarding copper complexes supported by symmetric ligands, **2a** ranges between $[Cu(MeCN)_2BPM]PF_6$ (**21**) and $[Cu(MeCN)_2DPM]PF_6$ (**0**). This indicates that pyrazole groups induce a higher catalytic activity than pyridine moieties in derived Cu(I) complexes and, by mixing these units, an intermediate activity results. As indicated by a TON of 9 exhibited by $[Cu(MeCN)_2BIMZ]PF_6$ (cf Scheme 9), imidazole appears to have an intermediate position between pyrazole and pyridine (cf. Table 1). Comparison of the asymmetric L_{py1} and the L_{imz1} systems, on the other hand, indicates that replacement of pyridine by imidazole may also decrease the activity of a derived copper(I) complex regarding the monooxygenation of 2,4-DTBP-H (see above).

Regarding the two other substrates, 3-TBP-H and 4-MeOP-H, comparison between the different catalysts is less straightforward due to the fact that oxygenation of these substrates is followed by an oxidative coupling reaction. The latter can also be copper-catalyzed;^[39, 40] the Cu(II) complex would thereby facilitate nucleophilic attack of the substrate (phenolate) onto the coordinated *ortho*-quinone and/or mediate the two-electron oxidation of the resulting catechol intermediate. Regarding the substrate 3-TBP-H we observed the so far highest TON (25) for **2a**, whereas that of **2b** (13) only reached about half of this value. This is again due to the steric hindrance of its methyl-substituted pyrazole unit. With the substrate 4-MeOP-H, on the other hand, both complexes **2a** and **2b** nearly reached the same TON (34 and 33, respectively) which in turn equals that of the most active catalysts $[Cu(MeCN)_2L_{imz1}]PF_6$ (**34**) and $[Cu(MeCN)_2BPM]PF_6$ (**35**). The other systems **dmBPM** (**15**) and **BIMZ** systems (**6**) achieve significantly lower TONs compared to **2a** and **2b**.

In summary, **2a** and **2b** show a high activity towards the substrates 3-TBP-H and 4-MeOP-H and a moderate activity towards 2,4-DTBP-H in comparison to other tyrosinase model systems supported by bidentate ligands. For monooxygenation of the last substrate the catalytic activity of Cu(I) complexes supported by ligands containing N-heterocyclic donor groups appears to follow the sequence pyrazole > imidazole \approx pyridine.

Homoleptic copper pyrazolylmethylpyridine complexes

In order to gain further information on the coordination behavior of the pyrazolylmethylpyridine ligands **1a** and **1b** towards copper(I) cations, crystal structures of the heteroleptic bis(acetonitrile) copper complexes **2a** and **2b** would be needed. For the analogous complexes with **BPM** and **dmBPM** structural

data are available.^[41, 42] However, determination of the molecular structure from crystals grown from a solution of **2a** showed that the homoleptic complex **3a** has formed (Figure 4, top). For **2b**, no crystals could be obtained. To further investigate the unexpected formation of **3a** and to also determine the structure of the missing analog **3b**, both **3a** and **3b** were directly synthesized by changing the ligand:metal stoichiometry to 2:1 (Scheme 4). By slow evaporation of the solvent suitable crystals for XRD were obtained, which allowed to determine the structure of the homoleptic complex **3b** (Figure 4, bottom).

The yellow copper(I) complex **3a** crystallizes in the monoclinic spacegroup $C2/c$ with four formula units per unit cell. The copper(I) cation is coordinated by two ligands of **1a** in a tetrahedrally-distorted geometry. N3-Cu1-N2 angles are $93.6(7)^\circ/93.2(3)^\circ$ within the chelating ligands and $108.4(5)^\circ/111.7(10)^\circ$ between the ligands. The average N-Cu-N angle is 110.0° . Metal-ligand bond distances are $1.993(18)$ Å for Cu-N_{py} (Cu1-N3) and $2.078(17)$ Å for Cu-N_{pz} (Cu1-N2), respectively. The second homoleptic copper(I) complex **3b** crystallizes in the monoclinic spacegroup $P2_1/n$ with four formula units per unit cell. The copper(I) cation is coordinated by two ligands **1b** in a tetrahedrally-distorted geometry. N-Cu-N angles are $94.22(7)^\circ$ (N2-Cu1-N3) and $92.99(7)^\circ$ (N23-Cu1-N22; both within chelating ligands) whereas the angles between ligands are $111.43(8)^\circ$ (N23-Cu1-N2) and $126.66(7)^\circ$ (N2-Cu1-N22). The average N-Cu-N angle is 119.0° . Metal-ligand bond distances are $2.0648(17)$ Å (Cu1-N3) and $2.0623(18)$ Å (Cu1-N23) for Cu-N_{py} as well as $2.0646(18)$ Å (Cu1-N2) and $2.0774(18)$ Å (Cu1-N22) for Cu-N_{pz}. The increase of the average N-Cu-N angle between two ligands from 110.0° in the **PMP** system (**3a**) to 119.0° in the methylated **dmPMP** system (**3b**) most likely derives from the increased steric hindrance. In comparison, the catalytic activity of the corresponding heteroleptic complexes **2a** and **2b** decreases with the introduction of the methyl groups.

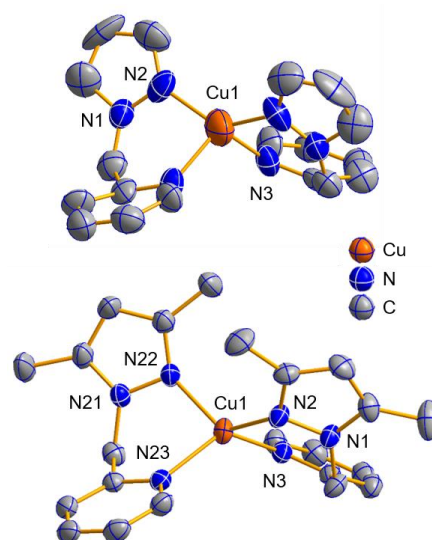


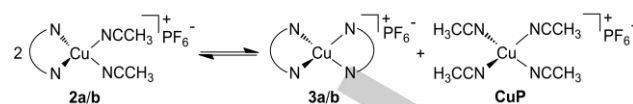
Figure 4. Crystal structure of $[Cu(PMP)_2]PF_6$ (**3a**, top), $[Cu(dmPMP)_2]PF_6$ (**3b**, bottom). Hydrogen atoms and PF_6 anions are omitted for better clarity. Selected crystal data and details on the structure refinements can be found in Table 4. In case of **3a**, the pyrazolyl and pyridinyl groups are disordered and **3a** and **3b** both crystallize as racemate (for details see Figure S22 and S23). Thermal ellipsoids are drawn with 50 % probability.

FULL PAPER

Equilibria between homo- and heteroleptic copper complexes

The fact that crystals of **3a** were obtained from a solution of **2a** suggests that the heteroleptic and homoleptic species are in equilibrium (Scheme 10). If this hypothesis was true, the concentration of the precatalysts **2a/b** according to Scheme 8 would be lowered, thus leading to a concomitant decrease of TON and TOF. This, however, only applies if the homoleptic complexes **3a/b** (and $[\text{Cu}(\text{MeCN})_4]\text{PF}_6$ **CuP**) are not catalytically active. In order to get more insight into this matter, it is essential to obtain information about the catalytic activities of every species involved in Scheme 10. Homoleptic complexes like **3a/b** would *a priori* be assumed to be catalytically inactive as their coordination environment does not support formation of a peroxy intermediate, in addition to the coordination of a substrate, without major rearrangement or loss of one ligand. Surprisingly, a test of the tyrosinase activities of the homoleptic systems **3a** and **3b** with 2,4-DTBP-H (Scheme 5) gave a different result; i.e., with a turnover number of 11 a significant catalytic activity was detected for **3a** (Table 2, cf. Figure S24 and S25). For **3b**, on the other hand, a relatively low TON of 6 was observed, even lower than that of the copper(I) precursor $[\text{Cu}(\text{MeCN})_4]\text{PF}_6$ (**CuP**; TON = 8; cf. Table 2 and Figure S26).^[24] Nevertheless this shows that, in addition to the heteroleptic complexes, also the homoleptic complexes and the pure precursor are catalytically active.

In case of an equilibrium between homo- and heteroleptic complexes (Scheme 10), it should be possible to generate the heteroleptic complexes **2a/b** by combining the homoleptic



Scheme 10. Equilibrium between hetero- (**2a/b**), homoleptic (**3a/b**) and precursor (**CuP**) Cu(I) complexes.

Table 2. Overview for the catalytic activity (TON) for the conversion of 2,4-DTBP-H to 3,5-DTQ under Bulkowski/Réglier conditions and UV/vis monitoring for heteroleptic complexes $[\text{Cu}(\text{MeCN})_2\text{PMP/dmPMP}]\text{PF}_6$ (**2a/b**), homoleptic systems $[\text{Cu}(\text{PMP/dmPMP})_2]\text{PF}_6$ (**3a/b**) and precursor complex $[\text{Cu}(\text{MeCN})_4]\text{PF}_6$ (**CuP**).

System	2a	3a	3a+CuP (1:1)	2b	3b	3b+CuP (1:1)	CuP
TON	14	11	13	11	6	7	8

complexes **3a/b** and the precursor complex $[\text{Cu}(\text{MeCN})_4]\text{PF}_6$ (**CuP**; Scheme 8, top). This was also observed by Garcia-Bosch and co-workers using bidentate imino-pyridine systems with a similar framework to investigate the mechanism of intramolecular hydroxylation of C-H-bonds in their complexes.^[43] However, in their case the homoleptic complex was not able to induce an hydroxylation and only the mono-ligated complex was reactive.^[43]

Following the example of Garcia-Bosch *et al.*, we applied a mixture of **3a/b** and $[\text{Cu}(\text{MeCN})_4]\text{PF}_6$ (**CuP**) in catalytic runs (Table 2; Figure S27, Figure S28).^[43] For the 1:1 combination of

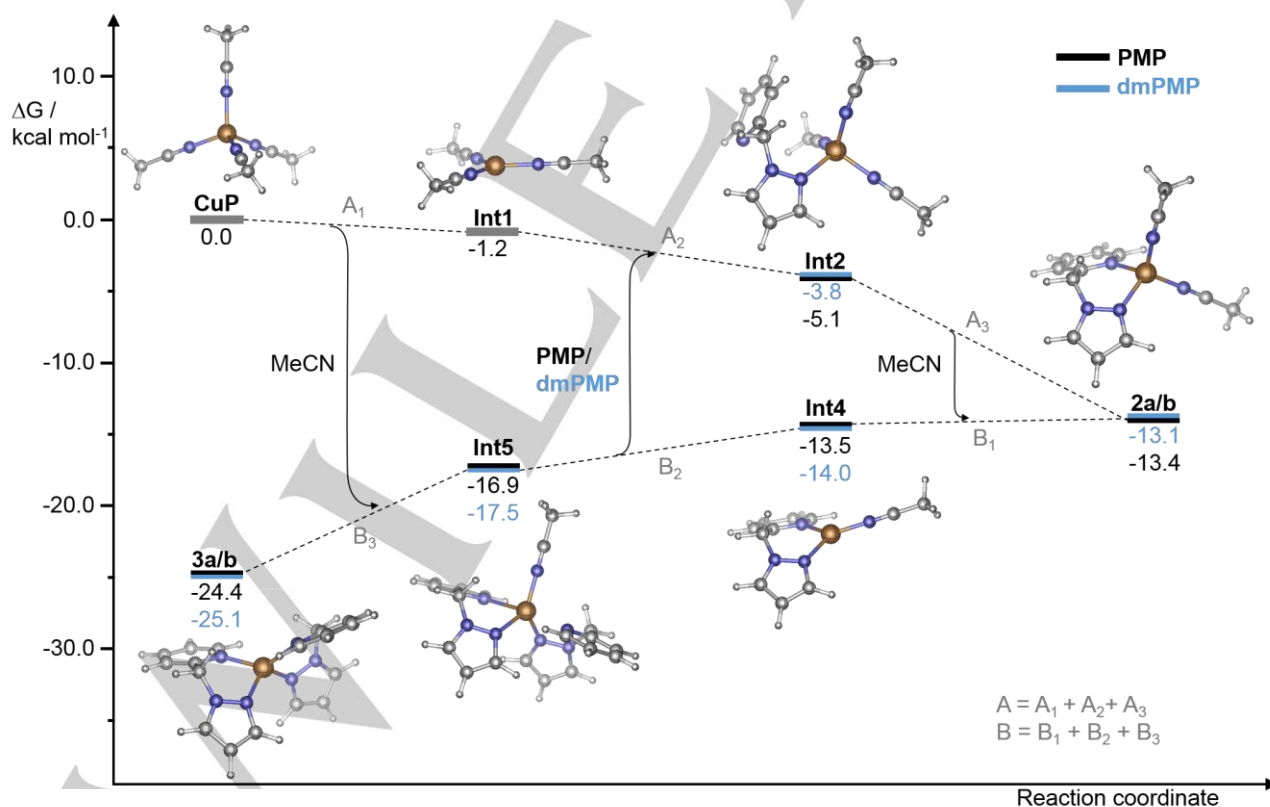


Figure 5. Theoretically calculated energy profile for the reaction between the hetero- and homoleptic PMP- and dmPMP-type catalysts $[\text{Cu}(\text{MeCN})_2\text{PMP}]\text{PF}_6$ (**2a**), $[\text{Cu}(\text{PMP})_2]\text{PF}_6$ (**3a**) and $[\text{Cu}(\text{MeCN})_2\text{dmPMP}]\text{PF}_6$ (**2b**), $[\text{Cu}(\text{dmPMP})_2]\text{PF}_6$ (**3b**). The molecules shown correspond to the PMP containing species. For better clarity the calculated intermediates **Int3** and **Int6** are omitted, which are not affecting the thermodynamics of the equilibrium (Scheme 10; for further details see Figure S29). Ligand exchange processes are shown by arrows.

FULL PAPER

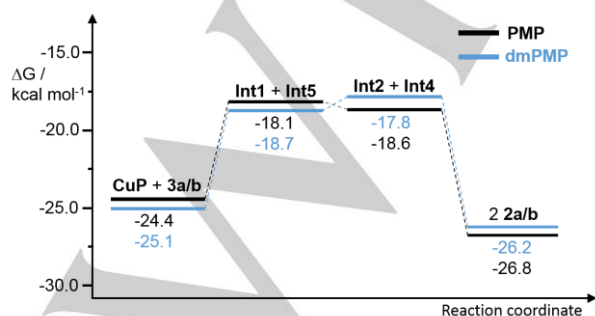
Table 3: Theoretically obtained Gibbs energies *G* for each individual step of the proposed equilibrium between hetero- and homoleptic **PMP**-type catalysts. The first number given always displays the values calculated for L = **PMP** and second number for L = **dmPMP**.

	Reaction	<i>G</i> / kcal mol ⁻¹
A ₁	[Cu(MeCN) ₄] ⁺ (CuP) → [Cu(MeCN) ₃] ⁺ (Int1) + MeCN	-1.2
A ₂	[Cu(MeCN) ₃] ⁺ (Int1) + L → [Cu(MeCN) ₃ L] ⁺ (Int2)	-3.9/-2.6
A ₃	[Cu(MeCN) ₃ L] ⁺ (Int2) → [Cu(MeCN) ₂ L] ⁺ (2a/b) + MeCN	-8.3/-9.3
A (A ₁ +A ₂ +A ₃)	[Cu(MeCN) ₄] ⁺ (CuP) + L → [Cu(MeCN) ₂ L] ⁺ (2a/b) + 2 MeCN	-13.4/-13.1
B ₁	[Cu(MeCN) ₂ L] ⁺ (2a/b) → [Cu(MeCN)L] ⁺ (Int4) + MeCN	-0.1/-0.9
B ₂	[Cu(MeCN)L] ⁺ (Int4) + L → [Cu(MeCN)LL] ⁺ (Int5)	-3.4/-3.5
B ₃	[Cu(MeCN)LL] ⁺ (Int5) → [CuL ₂] ⁺ (3a/b) + MeCN	-7.5/-7.6
B (B ₁ +B ₂ +B ₃)	[Cu(MeCN) ₂ L] ⁺ (2a/b) + L → [CuL ₂] ⁺ (3a/b) + 2 MeCN	-11.0/-12.0
B-A	2 [Cu(MeCN) ₂ L] ⁺ (2a/b) ⇌ [CuL ₂] ⁺ (3a/b) + [Cu(MeCN) ₄] ⁺ (CuP)	+2.4/+1.1

3a/b with **CuP** TONs of 13 and 7 were observed. In the presence of the equilibrium shown in Scheme 10 the catalytic activities of the mixtures should be equal to those observed in case of the heteroleptic complexes **2a** and **2b**. Indeed, for the **PMP**-system (**3a**) the value observed for **2a** (TON = 14) was almost reached, but in case of the **dmPMP**-system (**3b**), the activity (TON = 7) was found to be below the TON of **2b** (11; cf. Table 2). As the only difference between the two homoleptic **PMP**-type systems are the methyl substituents of the pyrazole, the greater steric bulk may hinder the formation of the heteroleptic complex.

To obtain further insight into the equilibrium between homo- and heteroleptic complexes shown in Scheme 10 DFT was employed. The computed reaction profiles shown in Figure 5 describe the formation of the heteroleptic complexes **2a/b** from the homoleptic complexes **3a/b** and precursor complex [Cu(MeCN)₄]PF₆ (**CuP**). The first step of the reaction involves the transfer of one acetonitrile ligand from **CuP** to the homoleptic complex **3a/b**, coupled to conversion of one bidentate ligand bound to the latter to a monodentate coordination mode (**Int5**). In the next step the κ⁻¹-bound ligand (**Int5**) dissociates and binds to the copper tris(acetonitrile) complex (**Int1**) to form **Int2**. This is followed by transfer of an acetonitrile molecule to the mono(acetonitrile) complex (**Int4**), ultimately forming two heteroleptic complexes **2a/b**.

The ligand exchange processes shown in Figure 5 can be separated into reaction sequences "A" (**CuP** to **2a/b**) and "B" (**2a/b** to **3a/b**) (cf. Table 1). Overall, the exchange reactions leading from **CuP** and **3a/b** to **2a/b** are almost isoergonic (line "B-A" in Table 1), in agreement with the observation of the equilibrium of Scheme 10. This is also evident from Figure 6 showing the combined energies of the species involved in Figure 5 along the reaction coordinate. As a matter of fact, a slightly more positive reaction enthalpy (+2.4 kcal/mol) is calculated for the for-

**Figure 6.** Reaction profile for the formation of **2a/b** from a mixture of homoleptic complex (**3a/b**) and copper precursor (**CuP**) and vice versa in compliance with Scheme 10.

mation of **3a** than for **3b** (+1.1 kcal/mol). This would indicate a slightly stronger preference for the heteroleptic complex **2a** than for its methylated analog **2b**. Methylation of the ligand thus should not influence the thermodynamics of the ligand exchange process. The fact that a lower TON is found by mixing **3b** and **CuP** in a 1:1 ratio than by applying pure **2b** indicates, however, that the picture may be more complicated. In the case of an attack of substrate and/or NEt₃ added for the catalytic runs on one of the intermediates shown in Figures 5 and 6, the condition of a "fast" pre-equilibrium to the catalytic cycle (which is implicitly assumed in the treatment of this Section; cf. Scheme 8) is not fulfilled any more, and additional reaction channels have to be considered.

Possible decomposition pathway of the catalyst

An important aspect of optimizing a catalyst is to explore all possibilities of increasing its efficiency and stability. Although we were able to improve the catalytic activity of some of our bidentate systems a complete conversion of the starting material to the desired *ortho*-quinone, corresponding to a TON of 100, was never achieved. We therefore also addressed the question of how the loss of activity takes place. Initially, we assumed that hydrolysis of the imine functions by water which forms during the catalytic cycle destroys the catalyst.^[23,24] Even though this might still be true for the systems bearing an imine function, the symmetric systems [Cu(MeCN)₂BPM]PF₆ or [Cu(MeCN)₂dmBPM]PF₆ showed a similar performance and the ligands themselves would not be affected by water.^[25] Therefore, hydrolysis cannot play the decisive role, and other deactivation processes might influence the catalysis.

In this context it is of interest that, by slow evaporation of a solution of **2b** in acetone after exposure to air, we were able to obtain blue crystals of the dinuclear Cu(II) complex [Cu₂(μ-F)(**1b**)₄](PF₆)₃ (**4**) representing a possible decay product of the catalyst (Figure 7). Compound **4** crystallizes in the monoclinic spacegroup C2/c with four formula units per unit cell. Similar to the homoleptic complex **3b** every copper(II) cation is coordinated by two **dmPMP** (**1b**) ligands. The two mononuclear Cu(**dmPMP**)₂ units are bridged by a fluoride anion to a dinuclear complex exhibiting C₂ symmetry. The coordination environment of each copper center can be described as distorted trigonal bipyramidal. The bridged fluoride anion located on the symmetry axis of the molecule shares a plane with four equatorial pyrazole N-donors at angles of F1-Cu1-N2 143.90(15)°, F1-Cu1-N22 111.42(15)° and N2-Cu1-N22 104.68(8)°. The axial positions are occupied with pyridine N-donors at a N3-Cu1-N23 angle of

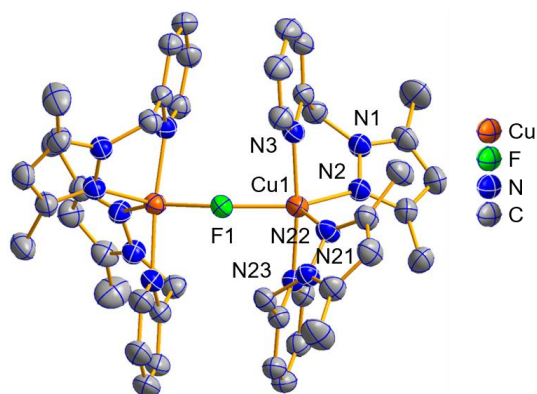


Figure 7. Crystal structure of $[\text{Cu}_2(\mu\text{-F})(\text{dmPMP})_4](\text{PF}_6)_3$ (**4**) (orange = Cu, grey = carbon, blue = nitrogen, red = oxygen, green-yellow = fluorine). Hydrogen atoms and PF_6^- anions are omitted for better clarity. Selected crystal data and details on the structure refinements can be found in Table 4. Thermal ellipsoids are drawn with 50 % probability.

$173.95(8)^\circ$. The angle between Cu1-F-Cu1 is $151.3(3)^\circ$. The bond distances for Cu-N_{pz} are $2.0284(19)$ Å (Cu1-N2), $2.1270(19)$ Å (Cu1-N22), for Cu-N_{py} $2.0094(19)$ Å (Cu1-N3) and $2.0167(19)$ Å (Cu1-N23) and for Cu1-F1 $1.9705(13)$ Å. The distance between the two copper cations is 3.818 Å.

The bridging fluoride atom in compound **4** has to be attributed to a decomposition of the PF_6^- anion. Importantly, formation of a similar dinuclear complex was observed for a copper(I) complex supported by tris[(2-pyridyl)methyl]amine ligand by Karlin and co-workers, where the reaction with oxygen led to the generation of mono- and dinuclear copper(II)fluorido complexes.^[44] Mono μ -fluorido bridged dimeric copper(II) complexes were also observed by Reger and co-workers with ditopic polypyrazolyl ligands.^[45] In these cases the bridging fluorido atoms originated from PF_6^- and BF_4^- anions, respectively.^[44,45] In future studies we will therefore examine the effect of more inert (and weakly coordinating)^[46] counterions on the stability and catalytic activity of small-molecule tyrosinase models.

Conclusions

In summary, we presented two new copper(I) complexes **2a** and **2b** capable of performing a tyrosinase-like monooxygenation reaction with the substrates 2,4-DTBP-H, 3-TBP-H and 4-MeOP-H. The TON for the pyridine-pyrazole mixed N-donor complex **2a** with the substrate 2,4-DTBP-H was 14, intermediate between the active **BPM** (22) and the inactive **DPM** system (0). This suggests that the electronic properties of a multidentate ligand can be designed in a modular fashion. In contrast to the moderate activity towards 2,4-DTBP-H, **2a** and **2b** exhibited high activities towards the substrates 3-TBP-H and 4-MeOP-H in comparison to other tyrosinase model systems. Moreover, we demonstrated experimentally and theoretically that the monoligated complexes **2a/b** are in an equilibrium with the homoleptic systems **3a/3b** which also exhibit some catalytic activity towards the substrate 2,4-DTBP-H. The crystal structure of a fluorido-bridged dicopper(II) complex is presented which may represent one of the possible decay products for the bidentate **PMP**-type ligand systems. This implies that use of a more inert anion than PF_6^- may lead to more robust catalytic systems.

Experimental Section

General procedures

Chemicals and solvents were purchased from Sigma-Aldrich Co. LLC, Deutero and Fisher Scientific in reagent grade. Dichloromethane and acetonitrile were further purified by heating to reflux over calcium hydride and distilled under a nitrogen atmosphere. Synthesis of the copper(I) complexes and preparation of the oxygenation mixtures were performed in a glovebox (MBraun, $\text{O}_2 < 1$ ppm; $\text{H}_2\text{O} < 1$ ppm). Column chromatography was carried out by using 0.04–0.063 mm mesh silica gel (Macherey-Nagel). R_f -values were determined by thin-layer chromatography on Polygram Sil G/UV254 (Macherey-Nagel, 0.2 mm particle size). NMR spectra were recorded at 300 K using a Bruker DRX 500 [^1H NMR (500.1 MHz), ^{13}C NMR (125.8 MHz)] and a Bruker AVANCE III HD Pulse Fourier Transform spectrometer operating at frequencies of 400.13 MHz (^1H), 100.62 MHz (^{13}C) with TMS as internal standard. The elemental analyses were performed using a Euro Vector CHNS-element analyser (Euro EA 3000): The prepared assays in tin vessels were burnt in a stream of oxygen. Infrared spectra were recorded on a Bruker ALPHA FT-IR Spectrum with a Platinum ATR setup. UV/vis measurements of the oxygenation mixtures were recorded in solution on an Agilent 8453 spectrometer by using a quartz cell with length $l = 1$ mm. Optical absorption spectra at low temperatures were recorded in solution on an Agilent Cary 5000 spectral photometer using a CryoVAC KONTI cryostat with a quartz cell length $l = 1$ cm. High resolution (HR) mass spectra were measured with an APEX 3 FT-ICR with an AccuTOF by Jeol (EI). Low-resolution mass spectra were measured with a MAT 8230 by Finnigan (EI), with a LCQ Classic by Thermo Finnigan (ESI) or an AutoflexSpeed by Bruker (MALDI-TOF).

Single-crystal structure determinations

Data collections were performed with an imaging plate diffraction system (IPDS-2) from STOE & CIE using $\text{Mo-K}\alpha$ -radiation. Structure solution was performed with SHELXT and structure refinement was performed against F^2 using SHELXL-2014. A numerical absorption correction was applied using programs X-RED and X-SHAPE as part of the program package X-Area. All non-hydrogen atoms were refined with anisotropic displacement parameters. The hydrogen atoms were positioned with idealized geometry (methyl H atoms allowed to rotate but not to tip) and were refined isotropic with $U_{\text{iso}}(\text{H}) = -1.2 U_{\text{eq}}(\text{C})$ (1.5 for methyl H atoms) using a riding model. In **3b** and **4** one hexafluorophosphate anion is disordered and was refined with a split model using partly restraints (SAME and SADI). In **3a** the cationic complex and the anion are disordered in two orientations in ratio 70:30. There are no hints for super structure reflections and if the structure is refined in space groups of lower symmetry, the disorder remain constant. Specific experimental details for growing of the crystals are described in the supporting information. CCDC-1566899 (**3a**), CCDC-1566901 (**3b**), CCDC-1566900 (**4**) contain the supplementary crystallographic data for this paper. These data can be obtained free charge from the Cambridge Crystallographic Data Centre via http://www.ccdc.cam.ac.uk/data_request/cif.

Computational Details

DFT calculations were performed with ORCA 4.0.1.^[47] The geometries of the two binuclear peroxo species studied by UV/vis spectroscopy were optimised by using the TPSSh functional^[48] and the Ahlrichs def2-TZVP basis set^[49] in conjunction with the chain of spheres approximation (RIJCOSX)^[50] and the general Ahlrichs Coulomb fitting basis set denoted def2/J.^[51] To account for dispersion effects Grimme's semiempirical dispersion correction scheme with Becke-Johnson damping (D3BJ)^[52] was used. The antiferromagnetic coupling between the copper centers was included via a broken symmetry wave function with one unpaired electron on each metal ion.

FULL PAPER

Table 4. Selected crystal data and details on the structure refinements for **3a**, **3b** and **4**.

	3a	3b	4
Formula	C ₁₈ H ₁₈ CuF ₆ N ₆ P	C ₂₂ H ₂₆ CuF ₆ N ₆ P	C ₄₄ H ₅₂ Cu ₂ F ₁₉ N ₁₂ P ₃
MW / g·mol ⁻¹	526.89	583.0	1329.96
Crystal system	monoclinic	monoclinic	monoclinic
Space group	C2/c	P2 ₁ /n	C2/c
a / Å	8.4065(4)	10.6322(3)	30.0652(8)
b / Å	20.5267(8)	21.9480(4)	9.8809(2)
c / Å	12.8749(6)	11.7581(3)	22.8798(6)
α / °	90	90	90
β / °	96.755(4)	93.847(3)	128.820(2)
γ / °	90	90	90
V / Å ³	2206.24(17)	115.852(2)	5295.6(3)
T / K	170(2)	170(2)	170(2)
Z	4	4	4
D _{calc} / mg·m ⁻³	1.586	1.568	1.668
μ / mm ⁻¹	1.130	1.018	1.008
θ _{max} / °	27.447	26.803	25.999
Refl. collected	16462	34767	27797
Unique reflections	2513	5273	5193
R _{int}	0.0587	0.0429	0.0285
Refl. [F ₀ >4σ(F ₀)]	2513	4725	4694
Parameters	287	365	427
R ₁ [F ₀ >4σ(F ₀)]	0.0428	0.0397	0.0376
wR ₂	0.1330	0.1040	0.0973
GOF	1.075	1.041	1.048
ρ _{max/min} / e·Å ⁻³	0.373/ -0.311	0.638/ -0.732	0.329/ -0.356

TD-DFT calculations were conducted with the same method except an addition of solvent effects with the conductor-like polarizable continuum model (CPCM)^[53] with acetone as solvent. For the UV/vis spectra the first 30 roots were computed.

All species included in the reaction profile study were optimized at the BP86/def2-SVP^[54, 49] level with dispersion correction (D3BJ) and resolution of identity (RIJ)^[55] with the fitting basis set def2J) in the gas phase. To account for basis set superposition errors in the geometries a geometrical counterpoise correction was employed.^[56] The identity of each structure as a minimum was verified via the absence of imaginary harmonic frequencies. These were obtained from frequency calculations which also provided thermochemical data. The enthalpy and entropy corrections to the electronic energy were taken for the computation of free enthalpies. The electronic energies for these were calculated with the DSD-BLYP double hybrid DFA^[57]. Therefore a large quadruple zeta basis set was employed (def2-QZVPP)^[49] as recommended by GRIMME *et al.*^[58]

To speed up the calculation density fitting was used for the correlation part as well for the coulomb and exchange integrals in combination with the chain of spheres approximation (RIJCOSX) and the appropriate fitting basis sets (def2-QZVPP/C^[59] and def2/J in ORCA terminology). To include solvation effects the SMD continuum solvation model (solvent dichloromethane) was applied to the electronic energies as it is parameterised to yield solvation free enthalpies.^[60]

General procedure for the oxygenation and quenching of external substrates for 2a and 2b

The copper(I) complex (1.25 μmol) was dissolved in 25 mL dichloromethane under an inert gas atmosphere resulting in a 500 μM solution. The monophenol (50 eq., 62.5 μmol) and triethylamine (100 eq., 0.125 mmol) were added. Subsequent injection of dioxygen at ambient temperature leads to the conversion to *ortho*-quinones, identified via UV/vis spectroscopy by absorption bands at the range of 390-425 nm. For the characterization of the formed products an aliquot (5 mL) was removed from the reaction mixture and diluted to a 100 μM solution in dichloromethane. This solution was treated with 6 M hydrochloric acid (20 mL) and the organic phase separated. The aqueous phase was extracted with dichloromethane (2x20 mL), the organic phases combined, dried over magnesium sulphate, filtered, and solvents evaporated in vacuum. The obtained residue was analysed via ¹H and ¹³C spectroscopy (see SI).

General procedure for the oxygenation of mixtures of 3a or 3b and [Cu(MeCN)₄]PF₆

The homoleptic copper(I) complex (0.625 μmol) and [Cu(MeCN)₄]PF₆ (0.625 μmol) were dissolved in dichloromethane (25 mL) under an inert gas atmosphere. 2,4-di-*tert*-butylphenol (100 eq., 62.5 μmol) and triethylamine (200 eq., 0.125 mmol) were added. Subsequent injection of dioxygen at ambient temperature lead to the conversion to *ortho*-quinones, identified via UV/vis spectroscopy by absorption bands at the range of 407 nm.

2-((1H-pyrazol-1-yl)methyl)pyridine (1a, PMP)

2-(Chloromethyl)pyridine hydrochloride (1.08 g, 6.58 mmol) and 1H-pyrazole (0.448 g, 6.58 mmol) were dissolved in toluene. A 40% aqueous sodium hydroxide solution (10 mL) and 40% aqueous tetrabutylammonium hydroxide (7 drops) were added and the resulting mixture was stirred and refluxed for 6 h. After cooling to room temperature, the solution was stirred overnight. The organic layer was separated, dried over magnesium sulphate, filtered and the solvent evaporated under reduced pressure. The crude product was purified by column chromatography on silica gel (cyclohexane/ethyl acetate, 1:2, R_f = 0.35) to obtain the desired product as a yellow oil (0.892 g, 5.59 mmol, 85%). Analytical data obtained were in accordance with the literature.^[29] IR (ATR): $\tilde{\nu}$ = 3110 (w), 3010 (w), 2937 (w), 1593 (m), 1573 (m), 1515 (m), 1475 (m), 1434 (m), 1394 (m), 1281 (w), 1149 (w), 1097 (m), 1049 (m), 993 (m), 965 (m), 747 (vs), 705 (s), 620 (s), 587 (m) cm⁻¹. ¹H NMR (500 MHz, CDCl₃, 300 K): δ = 8.56 (ddd, ³J = 4.8, ⁴J = 1.6, ⁵J = 0.8 Hz, 1 H, C_{py-H6}), 7.62 (td, ³J = 7.7, ⁴J = 1.8 Hz, 1 H, C_{py-H4}), 7.57 (d, ³J = 1.5 Hz, 1 H, C_{pz-H3}), 7.52 (d, ³J = 2.3 Hz, 1 H, C_{pz-H5}), 7.20 – 7.15 (m, 1 H, C_{py-H5}), 6.96 (d, ³J = 7.9 Hz, 1 H, C_{py-H3}), 6.31 (t, ³J = 2.1 Hz, 1 H, C_{pz-H4}), 5.45 (s, 2 H, CH₂) ppm. ¹³C NMR (126 MHz, CDCl₃, 300 K): δ = 156.9 (C_{py-2}), 149.5 (C_{py-6}), 140.1 (C_{pz-3}), 137.2 (C_{py-4}), 130.1 (C_{pz-5}), 122.8 (C_{py-5}), 121.8 (C_{py-3}), 106.3 (C_{pz-4}), 57.6 (CH₂) ppm. HR-MS (EI): m/z [M]⁺ calcd. for C₉H₉N₃, 159.0797; found 159.0803. MS (EI, 70 eV): m/z (%) = 159.08 [M]⁺, 92.05 [M-pz]⁺.

FULL PAPER

2-((3,5-dimethyl-1H-pyrazol-1-yl)methyl)pyridine (**1b**, dmPMP)

Compound **1b** was prepared in a similar manner as described for **1a** using 2-(chloromethyl)pyridine hydrochloride (2.16 g, 13.2 mmol) and 3,5-dimethyl-1H-pyrazole (1.27 g, 13.2 mmol). The crude product was purified by column chromatography on silica gel (ethyl acetate, R_f = 0.31) to obtain the desired product as a yellow oil (1.71 g, 9.13 mmol, 69%). Analytical data obtained were in accordance with the literature.^[29] IR (ATR): $\tilde{\nu}$ = 3109 (w), 3054 (w), 3014 (w), 2939 (w), 1593 (m), 1572 (m), 1511 (m), 1476 (m), 1432 (m), 1394 (s), 1355 (m), 1277 (m), 1215 (w), 1150 (w), 1088 (m), 1049 (s), 995 (m), 966 (m), 915 (w), 748 (vs), 705 (s), 621 (s) cm⁻¹. ¹H NMR (500 MHz, CDCl₃, 300 K): δ = 8.53 (ddd, ³J = 4.9, ⁴J = 1.7, ⁵J = 0.9 Hz, 1 H, C_{py}-H6), 7.62 (td, ³J = 7.7, ⁴J = 1.8 Hz, 1 H, C_{py}-H4), 7.18 – 7.11 (m, 1 H, C_{py}-H5), 6.77 (d, ³J = 7.9 Hz, 1 H, C_{py}-H3), 5.86 (s, 1 H, C_{pz}-H4), 5.32 (s, 2 H, CH₂), 2.24 (s, 3 H, C_{pz}3-CH₃), 2.16 (s, 3 H, C_{pz}5-CH₃) ppm. ¹³C NMR (126 MHz, CDCl₃, 300 K): δ = 157.6 (C_{py}-2), 149.4 (C_{py}-6), 148.2 (C_{pz}-3), 139.8 (C_{pz}-5), 137.2 (C_{py}-4), 122.5 (C_{py}-5), 121.0 (C_{py}-3), 105.8 (C_{pz}-4), 54.5 (CH₂), 13.6 (C_{pz}3-CH₃), 11.2 (C_{pz}5-CH₃) ppm. HR-MS (EI): m/z [M]⁺ calcd. for C₁₁H₁₃N₃, 187.1110; found 187.1160. MS (EI, 70 eV): m/z (%) = 187.11 [M]⁺, 109.08 [M-C₅H₄N]⁺, 93.05 [M-pz+H]⁺.

[Cu(MeCN)₂(PMP)]PF₆ (**2a**)

Tetrakis(acetonitrile)copper(I) hexafluorophosphate (259 mg, 0.694 mmol) was dissolved in 6 mL dry acetonitrile and a 8 mL solution of **1a** (110 mg, 0.694 mmol) in dry acetonitrile was slowly added via a syringe. The resulting yellow solution was stirred for 30 min at room temperature and the solvent evaporated. The desired product was obtained as a yellow solid (161 mg, 0.358 mmol, 52%). IR (ATR): $\tilde{\nu}$ = 3133 (w), 2941 (w), 2302 (w), 2276 (w), 1600 (w), 1477 (w), 1432 (m), 1403 (m), 1309 (w), 1275 (w), 1165 (w), 1091 (w), 1066 (w), 826 (vs), 778 (s), 751 (s), 705 (m), 620 (m), 556 (s), 482 (m), 448 (m) cm⁻¹. ¹H NMR (500 MHz, [D₆]acetone, 300 K): δ = 8.68 (d, ³J = 4.9, 1 H, C_{py}-H6), 8.11 – 8.06 (m, 2 H, C_{py}-H4, C_{pz}-H3), 7.83 (d, ³J = 7.7 Hz, 1 H, C_{py}-H3), 7.75 (d, ³J = 1.9 Hz, 1 H, C_{pz}-H5), 7.61 (ddd, ³J = 7.6, ³J = 5.1, ⁴J = 0.9 Hz, 1 H, C_{py}-H5), 6.46 (t, ³J = 2.3 Hz, 1 H, C_{pz}-H4), 5.69 (s, 2 H, CH₂), 2.28 (s, 6 H, NCCH₃) ppm. ¹³C NMR (126 MHz, [D₆]acetone, 300 K): δ = 154.5 (C_{py}-2), 151.1 (C_{py}-6), 141.8 (C_{pz}-3), 140.4 (C_{py}-4), 133.1 (C_{pz}-5), 126.1 (C_{py}-5), 125.9 (C_{py}-3), 118.2 (NCCH₃), 107.1 (C_{pz}-4), 55.9 (CH₂), 1.71 (NCCH₃) ppm. MS (MALDI-TOF): m/z (%) = 222.1 (100) [M – 2 NCCH₃ – PF₆]⁺, 262.9 (76) [M – NCCH₃ – PF₆]⁺. C₁₃H₁₅CuF₆N₅P (449.8): calcd. C 34.71, H 3.36, N 15.57; found C 34.55, H 3.56, N 15.45.

[Cu(MeCN)₂(dmPMP)]PF₆ (**2b**)

Compound **2b** was prepared in a similar manner as described for **2a** using Tetrakis(acetonitrile)copper(I) hexafluorophosphate (219 mg, 0.587 mmol) and **1b** (110 mg, 0.587 mmol). The desired product was obtained as a yellow solid (160 mg, 0.335 mmol, 57%). IR (ATR): $\tilde{\nu}$ = 2950 (w), 2278 (w), 1601 (w), 1553 (m), 1474 (m), 1431 (m), 1393 (m), 1315 (w), 1280 (w), 1158 (w), 1056 (w), 829 (vs), 768 (s), 679 (m), 606 (m), 556 (s), 479 (m), 415 (m) cm⁻¹. ¹H NMR (400 MHz, [D₆]acetone, 300 K): δ = 8.65 (ddd, ³J = 5.1, ⁴J = 1.6, ⁵J = 0.8 Hz, 1 H, C_{py}-H6), 8.09 (td, ³J = 7.7, ⁴J = 1.7 Hz, 1 H, C_{py}-H4), 7.92 – 7.86 (m, 1 H, C_{py}-H3), 7.60 (ddd, ³J = 7.7, ³J = 5.1, ⁴J = 1.3 Hz, 1 H, C_{py}-H5), 6.06 (s, 1 H, C_{pz}-H4), 5.44 (s, 2 H, CH₂), 2.45 (s, 3 H, C_{pz}3-CH₃), 2.30 (s, 6 H, NCCH₃), 2.21 (s, 3 H, C_{pz}5-CH₃) ppm. ¹³C NMR (101 MHz, [D₆]acetone, 300 K): δ = 154.5 (C_{py}-2), 151.1 (C_{py}-6), 149.8 (C_{pz}-3), 142.6 (C_{pz}-5), 140.5 (C_{py}-4), 126.1 (C_{py}-5), 125.8 (C_{py}-3), 118.4 (NCCH₃), 106.6 (C_{pz}-4), 52.4 (CH₂), 13.8 (C_{pz}3-CH₃), 11.1 (C_{pz}5-CH₃), 1.77 (NCCH₃) ppm. MS (MALDI-TOF): m/z (%) = 250.2 (100) [M – 2 NCCH₃ – PF₆]⁺, 290.9 (43) [M – NCCH₃ – PF₆]⁺. C₁₅H₁₉CuF₆N₅P (477.9): calcd. C 37.70, H 4.01, N 14.66; found C 37.40, H 4.30, N 14.27.

[Cu(PMP)₂]PF₆ (**3a**)

Tetrakis(acetonitrile)copper(I) hexafluorophosphate (135 mg, 0.361 mmol) was dissolved in 6 mL dry acetonitrile and slowly added to a 4 mL solution of **1a** (135 mg, 0.722 mmol) in dry acetonitrile via a syringe. The resulting yellow solution was stirred for 30 min at room temperature and the solvent evaporated. The desired product was obtained as a yellow solid (160 mg, 0.304 mmol, 84%). IR (ATR): $\tilde{\nu}$ = 3137 (w), 1600 (w), 1430 (m), 1403 (w), 1309 (w), 1275 (w), 1162 (w), 1093 (w), 1063 (w), 979 (w), 830 (s), 779 (m), 749 (s), 705 (m), 620 (m), 557 (s), 470 (w) cm⁻¹. ¹H NMR (400 MHz, [D₆]acetone, 300 K): δ = 8.59 (s, 2 H, C_{py}-H6), 8.10 – 8.06 (m, 4 H, C_{py}-H4, C_{pz}-H3), 7.89 (s, 2 H, C_{py}-H3), 7.70 (s, 2 H, C_{pz}-H5), 7.55 (s, 2 H, C_{py}-H5), 6.46 (s, 2 H, C_{pz}-H4), 5.81 (s, 4 H, CH₂) ppm. ¹³C NMR (101 MHz, [D₆]acetone, 300 K): δ = 154.7 (C_{py}-2), 150.8 (C_{py}-6), 141.1 (C_{pz}-3), 139.6 (C_{py}-4), 132.4 (C_{pz}-5), 126.0 (C_{py}-5), 125.9 (C_{py}-3), 107.0 (C_{pz}-4), 56.4 (CH₂) ppm. MS (ESI⁺, CHCl₃): m/z = 381.2 [M-PF₆]⁺, 222.2 [M-PF₆-PMP]⁺. C₁₈H₁₈CuF₆N₆P (526.9): calcd. C 41.03, H 3.44, N 15.95; found C 41.16, H 3.32, N 15.70.

[Cu(dmPMP)₂]PF₆ (**3b**)

Compound **3b** was prepared in a similar manner as described for **3a** using Tetrakis(acetonitrile)copper(I) hexafluorophosphate (148 mg, 0.396 mmol) and **1b** (126 mg, 0.792 mmol). The desired product was obtained as a yellow solid (144 mg, 0.247 mmol, 62%). IR (ATR): $\tilde{\nu}$ = 2920 (w), 1599 (w), 1550 (w), 1472 (m), 1417 (m), 1389 (m), 1315 (m), 1285 (w), 1224 (w), 1060 (w), 1043 (w), 1009 (w), 817 (s), 774 (s), 681 (m), 629 (w), 598 (m), 554 (s), 477 (m), 415 (m) cm⁻¹. ¹H NMR (400 MHz, [D₃]acetonitrile, 300 K): δ = 8.36 (s, 2 H, C_{py}-H6), 7.88 (t, ³J = 7.3 Hz, 2 H, C_{py}-H4), 7.51 (d, ³J = 7.3 Hz, 2 H, C_{py}-H3), 7.37 (m, 2 H, C_{py}-H5), 5.95 (s, 2 H, C_{pz}-H4), 5.26 (s, 4 H, CH₂), 2.34 (s, 6 H, C_{pz}3-CH₃), 2.00 (s, 6 H, C_{pz}5-CH₃) ppm. ¹³C NMR (101 MHz, [D₃]acetonitrile, 300 K): δ = 155.4 (C_{py}-2), 150.6 (C_{py}-6), 149.1 (C_{pz}-3), 141.8 (C_{pz}-5), 139.3 (C_{py}-4), 125.3 (C_{py}-5), 125.1 (C_{py}-3), 106.6 (C_{pz}-4), 53.5 (CH₂), 13.7 (C_{pz}3-CH₃), 11.4 (C_{pz}5-CH₃) ppm. MS (ESI⁺, acetonitrile): m/z = 437.2 [M-PF₆]⁺, 250.2 [M-PF₆-dmPMP]⁺. C₂₂H₂₆CuF₆N₆P (583.0): calcd. C 45.32, H 4.50, N 14.42; found C 45.62, H 4.50, N 14.25.

[Cu₂(μ-F)(dmPMP)₄](PF₆)₃ (**4**)

A 3 mM solution of **2b** in 3 mL acetone was exposed to air and the solvent slowly evaporated. After four weeks small blue crystals of (**4**) suitable for X-ray structure determination were obtained.

Acknowledgements

The authors thank Deutsche Forschungsgemeinschaft (Tu58/15-1) and CAU Kiel for financial support of this research.

Keywords: type 3 copper enzyme • tyrosinase • dioxygen activation • catalysis • N-donor ligands

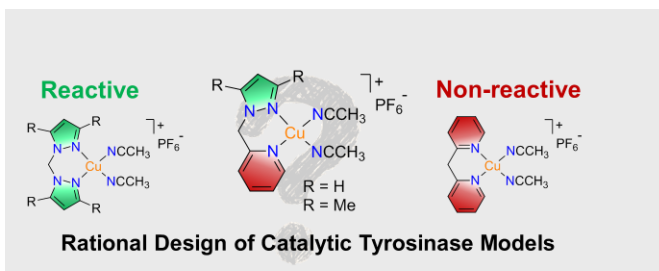
- [1] a) G. Prota, *Med. Res. Rev.* **1988**, *8*, 525-556.; b) Y. J. Kim, H. Uyama, *Cell. Mol. Life Sci.* **2005**, *62*, 1707-1723.
 [2] a) J.-S. Taylor, *Science* **2015**, *347*, 824.; b) C. Olivares, F. Solano, *Pigment Cell Melanoma Res.* **2009**, *22*, 750.; c) E. Dadachova, R. A. Bryan, X. Huang, T. Moadel, A. D. Schweitzer, P. Aisen, J. D. Nosanchuk, A. Casadevall, *PLoS ONE* **2007**, *2*, e457.
 [3] a) C. J. Coates, J. Nairn, *Dev. Comp. Immunol.* **2014**, *38*, 43-55.; b) L. Cerenius, K. Söderhäll, *Immunol. Rev.* **2004**, *198*, 116-126.; c) H. Decker, E. Jaenicke, *Dev. Comp. Immunol.* **2004**, *28*, 673-87.
 [4] a) A. Gibbons, *Science* **2014**, *346*, 934-936.; b) R. A. Spritz, J. Oh, K. Fukui, S. A. Holmes, L. Ho, D. Chitayat, T. D. France, M. A. Musarella, S. J. Orlov, R. E. Schnur, R. G. Weleber, A. V. Levin, *Human Mutat.* **1997**, *10*, 171-174.
 [5] M. R. Loizzo, R. Tundis, F. Menichini, *Compr. Rev. Food Sci. Food Saf.* **2012**, *11*, 378-398.

FULL PAPER

- [6] a) E. I. Solomon, D. E. Heppner, E. M. Johnston, J. W. Ginsbach, J. Cirera, M. Qayyum, M. T. Kieber-Emmons, C. H. Kjaergaard, R. G. Hadt and L. Tian, *Chem. Rev.* **2014**, *114*, 3659–3853.; b) C. E. Elwell, N. L. Gagnon, B. D. Neisen, D. Dhar, A. D. Spaeth, G. M. Yee, W. B. Tolman, *Chem. Rev.* **2017**, *117* (3), 2059–2107.
- [7] M. Rolff, J. Schottenheim, H. Decker, F. Tuczek, *Chem. Soc. Rev.* **2011**, *40*, 4077–4098.
- [8] J. N. Hamann, B. Herzigkeit, R. Jurgeleit, F. Tuczek, *Coord. Chem. Rev.* **2017**, *334*, 54–66.
- [9] E. I. Solomon, U. M. Sundaram, T. E. Machonkin, *Chem. Rev.* **1996**, *96*, 2563–2606.
- [10] Y. Matoba, T. Kumagai, A. Yamamoto, H. Yoshitsu, M. Sugiyama, *J. Biol. Chem.* **2006**, *281*, 8981–8990.
- [11] a) M. Sendovski, M. Kanteev, V. S. Ben-Yosef, N. Adir, A. Fishman, *J. Mol. Biol.* **2011**, *405*, 227–237.; b) W. T. Ismaya, H. J. Rozeboom, A. Weijin, J. J. Mes, F. Fusetti, H. J. Wichers, B. W. Dijkstra, *Biochemistry* **2011**, *50*, 5477–5486.; c) N. Fujieda, S. Yabuta, T. Ikeda, T. Oyama, N. Muraki, G. Kurisu, S. Itoh, *J. Biol. Chem.* **2013**, *288*, 22128–22140.; d) A. Bijelic, M. Pretzler, C. Molitor, F. Zekiri, A. Rompel, *Angew. Chem. Int. Ed.* **2015**, *54*, 14677–14680.
- [12] a) M. Goldfeder, M. Kanteev, S. Isaschar-Ovdat, N. Adir, A. Fishman, *Nat. Commun.* **2014**, *5*, 4505.; b) M. Kanteev, M. Goldfeder, A. Fishman, *Protein Sci.* **2015**, *24*, 1360–1369.
- [13] E. Solem, F. Tuczek, H. Decker, *Angew. Chem.* **2016**, *128*, 2934–2938.
- [14] I. Garcia-Bosch, R. Cowley, D. E. Diaz, E. I. Solomon, K. D. Karlin, *J. Am. Chem. Soc.* **2017**, *139* (8), 3186–3195.
- [15] a) P. Zerón, M. Westphal, P. Comba, M. Flores-Álamo, A. C. Stueckl, C. Leal-Cervantes, V. M. Ugalde-Saldívar, L. Gasque, *Eur. J. Inorg. Chem.* **2017**, *1*, 56–62.; b) P. Comba, C. Haaf, S. Helmle, K. D. Karlin, S. Pandian, A. Waleska, *Inorg. Chem.* **2012**, *51* (5), 2841–2851.
- [16] a) I. A. Koval, K. Selmecci, C. Belle, C. Philouze, E. Saint-Aman, I. Gautier-Luneau, A. M. Schuitema, M. van Vliet, P. Gamez, O. Roubeau, M. Lünen, B. Krebs, M. Lutz, A. L. Speck, J.-L. Pierre, J. Reedijk, *Chem. Eur. J.* **2006**, *12*, 6138–6150.; b) I. A. Koval, P. Gamez, C. Belle, K. Selmecci, J. Reedijk, *Chem. Soc. Rev.* **2006**, *35*, 814–840.
- [17] S. K. Dey, A. Mukherjee, *Coord. Chem. Rev.* **2016**, *310*, 80–115.
- [18] M. Réglier, C. Jorand, B. Wagell, *J. Chem. Soc. Chem. Commun.* **1990**, *24*, 1752–1755.
- [19] L. Casella, M. Gullotti, M. Bartosek, G. Pallanza, E. Laurenti, *J. Chem. Soc. Chem. Commun.* **1991**, *18*, 1235–1237.
- [20] G. Battaini, M. De Carolis, E. Monzani, F. Tuczek, L. Casella, *Chem. Commun.* **2003**, *6*, 726–727.
- [21] L. M. Mirica, M. Vance, D. J. Rudd, B. Hedman, K. O. Hodgson, E. I. Solomon, T. D. P. Stack, *Science* **2005**, *308*, 1890–1892.
- [22] a) K. V. N. Esguerra, Y. Fall, J.-P. Lumb, *Angew. Chem. Int. Ed.* **2014**, *53*, 5877.; b) M. S. Askari, K. V. N. Esguerra, J.-P. Lumb, X. Ottenwaelder, *Inorg. Chem.* **2015**, *54*, 8665–8762.; c) K. V. N. Esguerra, J.-P. Lumb, *Synlett.* **2015**, *26*, 2731–2738.
- [23] M. Rolff, J. Schottenheim, G. Peters, F. Tuczek, *Angew. Chem. Int. Ed.* **2010**, *49*, 6438–6442.
- [24] a) J. Schottenheim, N. Fateeva, W. Thimm, J. Krahrmer, F. Tuczek, *Z. Allg. Anorg. Chem.* **2013**, *8*, 1491–1497.; b) J. N. Hamann, F. Tuczek, *Chem. Commun.* **2014**, *50*(18), 2298–2300.
- [25] J. N. Hamann, R. Schneider, F. Tuczek, *J. Coord. Chem.* **2015**, *68*(17–18), 3259–3271.
- [26] F. Wendt, C. Näther, F. Tuczek, *J. Biol. Inorg. Chem.* **2016**, *21*(5–6), 777–792.
- [27] A. Hoffmann, C. Citek, S. Binder, A. Goos, M. Rübhausen, O. Troepfner, I. Ivanović-Burmazović, E. C., Wasinger, T. D. P. Stack, S. Herres-Pawlis, *Angew. Chem. Int. Ed.* **2013**, *52*, 5398–5401.
- [28] a) S. O. Ojwach, I. A. Guzei, L. L. Benade, S. F. Mapolie, J. Darkwa, *Organometallics* **2009**, *28*, 2127–2133.; b) S. O. Ojwach, T. T. Okemwa, N. W. Attandoha, B. Omondic, *Dalton Trans.* **2013**, *42*, 10735.; c) F. A. Mautner, C. Berger, M. J. Dartez, Q. L. Nguyen, J. Favreau, S. S. Massoud, *Polyhedron* **2014**, *69*, 48–54.
- [29] D. A. House, P. J. Steel, A. A. Watson, *Aust. J. Chem.* **1986**, *39*, 1525–1536.
- [30] R. Gupta, T. K. Lal, R. Mukherjee, *Polyhedron* **2002**, *21* (12–13), 1245–1253.
- [31] J. E. Bulkowski, *United States Patent 4.545.937* **1985**, Oct. 8.
- [32] A. E. M. M. Ramadan, S. Youssef, H. Eissa, *Int. J. Adv. Res.* **2014**, *2*(8), 116–130.
- [33] M. J. Nilges, H. M. Swartz, P. A. Riley, *J. Biol. Chem.* **1984**, *259* (4), 2446–2451.
- [34] O. Reinaud, P. Capdevielle, M. Maumy, *Tetrahedron Lett.* **1985**, *26*(33), 3993–3996.
- [35] In previous publications the TONs with **BPM** and **dmBPM** for the substrates 3-TBP-H and 4-MeOP-H were calculated for the primarily formed *ortho*-quinones. As these actually form secondary products (coupled *ortho*-quinones) we corrected the TONs.
- [36] K. Fujisawa, T. Ono, Y. Ishikawa, N. Amir, Y. Miyashita, K. Okamoto, N. Lehnert, *Inorg. Chem.* **2006**, *45*, 1698–1713.
- [37] a) C. Wilfer, P. Liebhäuser, A. Hoffmann, H. Erdmann, O. Grossmann, L. Runtsch, E. Paffenholz, R. Schepper, R. Dick, S. Herres-Pawlis, *Chem. Eur. J.* **2015**, *21*, 17639–17649.; b) C. Wilfer, P. Liebhäuser, H. Erdmann, A. Hoffmann, S. Herres-Pawlis, *Eur. J. Inorg. Chem.* **2015**, *3*, 494–502.; c) P. Liebhäuser, K. Keisers, A. Hoffmann, T. Schnappinger, I. Sommer, A. Thoma, C. Wilfer, R. Schoch, K. Stührenberg, M. Bauer, M. Dürr, I. Ivanović-Burmazović, S. Herres-Pawlis, *Chem. Eur. J.* **2017**, *23*, 1–13.
- [38] G. J. Karahalīs, A. Thangavel, B. Chica, J. Bacsa, R. B. Dyer, C. C. Scarborough, *Inorg. Chem.* **2016**, *55* (3), 1102–1107.
- [39] L. M. Sayre, D. V. Nadkarni, *J. Am. Chem. Soc.* **1994**, *116*, 3157–3158.
- [40] L. Casella, E. Monzani, M. Gullotti, D. Cavagnino, G. Cerina, L. Santagostini, R. Ugo, *Inorg. Chem.* **1996**, *35* (26), 7516–7525.
- [41] C.-C. Chou, C.-C. Su, H.-L. Tsai, K.-H. Lii, *Inorg. Chem.* **2005**, *44*, 628–632.
- [42] M. J. Calhorda, P. J. Costa, O. Crespo, M. C. Gimeno, P. G. Jones, A. Laguna, M. Naranjo, S. Quintal, Y.-J. Shia, M. D. Villacampa, *Dalton Trans.* **2006**, *34*, 4104–4113.
- [43] R. Trammell, Y. Y. See, A. T. Herrmann, N. Xie, D. E. Diaz, M. A. Siegler, P. S. Baran, I. Garcia-Bosch, *J. Org. Chem.* **2017**, *82* (15), 7887–7904.
- [44] R. R. Jacobson, Z. Tyeklar, K. D. Karlin, J. Zubietta, *Inorg. Chem.* **1991**, *30*, 2035–2040.
- [45] a) D. L. Reger, E. A. Foley, R. P. Watson, P. J. Pellechia, M. D. Smith, F. Grandjean, G. J. Long, *Inorg. Chem.* **2009**, *48*, 10658–10669.; b) D. L. Reger, A. E. Pascui, M. D. Smith, J. Jezierska, A. Ozarowski, *Inorg. Chem.* **2012**, *51*, 11820–11836.; c) D. L. Reger, A. E. Pascui, P. J. Pellechia, A. Ozarowski, *Inorg. Chem.* **2013**, *52*, 12741–12748.
- [46] I. M. Riddlestone, A. Kraft, J. Schaefer, I. Krossing, *Angew. Chem.* **2017**, DOI: 10.1002/ange.2017110782.
- [47] F. Neese, *WIREs Comput. Mol. Sci.* **2012**, *2*, 73.
- [48] J. M. Tao, J. P. Perdew, V. N. Staroverov, G. E. Scuseria, *Phys. Rev. Lett.* **2003**, *91*, 146401.
- [49] F. Weigend, R. Ahlrichs, *Phys. Chem. Chem. Phys.* **2005**, *7*, 3297.
- [50] F. Neese, F. Wennmohs, A. Hansen, U. Becker, *Chem. Phys.* **2009**, *356*, 98–109.
- [51] F. Weigend, *Phys. Chem. Chem. Phys.* **2006**, *8*, 1057–1065.
- [52] (a) S. Grimme, *J. Comput. Chem.* **2004**, *25*, 1463–1473. (b) S. Grimme, *J. Comput. Chem.* **2006**, *27*, 1787–1799. (c) S. Grimme, S. Ehrlich, L. Goerigk, *J. Comput. Chem.* **2011**, *32*, 1456–1465. (d) S. Grimme, J. Antony, S. Ehrlich, H. Krieg, *J. Chem. Phys.* **2010**, *132*, 154104.
- [53] V. Barone, M. Cossi, *J. Phys. Chem. A* **1998**, *102*, 1995.
- [54] a) A. D. Becke, *Phys. Rev. A* **1988**, *38*, 3098–3100.; b) J. P. Perdew, *Phys. Rev. B* **1986**, *33*, 8822–24.
- [55] a) K. Eichkorn, H. Treutler, H. Öhm, M. Häser, R. Ahlrichs, *Chem. Phys. Lett.* **1995**, *240*, 283–290.; b) K. Eichkorn, F. Weigend, O. Treutler, R. Ahlrichs, *Theor. Chem. Acc.* **1997**, *97*, 119–124.; c) F. Neese, *J. Comput. Chem.* **2003**, *24*, 1740–1747.
- [56] H. Kruse, S. Grimme, *J. Chem. Phys.* **2012**, *16*, 136.
- [57] S. Kozuch, D. Gruzman, J. M. L. Martin, *J. Phys. Chem. C* **2010**, *114*, 20801–20808.
- [58] L. Goerigk, A. Hansen, C. Bauer, S. Ehrlich, A. Najibi, S. Grimme, *Phys. Chem. Chem. Phys.* **2017**, *19*, 32184–32215.
- [59] A. Hellweg, C. Hattig, S. Hofener, W. Klopper, *Theor. Chem. Acc.* **2007**, *117*, 587.
- [60] A. V. Marenich, C. J. Cramer, D. G. Truhlar, *J. Phys. Chem. B* **2009**, *113*, 6378.

FULL PAPER

FULL PAPER



One pyrazole makes the difference. We studied copper(I) complexes supported by bidentate ligands containing a combination of pyridine and pyrazole units regarding their tyrosinase activity towards various monophenols. The properties of the heteroleptic complexes and their homoleptic counterparts are elucidated by experimental and theoretical studies.

Copper Tyrosinase Models

*Benjamin Herzigkeit, Benedikt M. Flöser,
Tobias A. Engesser, Christian Näther
and Felix Tuczek*

Page No. – Page No.

Tyrosinase model systems supported by pyrazolymethylpyridine ligands: electronic and steric factors influencing the catalytic activity and impact of complex equilibria in solution